Int. J. Electrochem. Sci., 14 **(2019)** 6628 – 6642, doi: 10.20964/2019.07.39

International Journal of
ELECTROCHEMICAL
SCIENCE
www.electrochemsci.org

Well-dispersed Amorphous Ta_2O_5 Chemically Grafted onto Multi-Walled Carbon Nanotubes for High-performance Lithium Sulfur Battery

Ziqiong Li, Jie Xu, Juan Wang, Dongfang Niu[*]*, Shuozhen Hu, Xinsheng Zhang*[*]

State Key Laboratory of Chemical Engineering, East China University of Science and Technology, Shanghai, 200237, China
[*]E-mail: dfniu@ecust.edu.cn, xszhang@ecust.edu.cn

Received: 1 March 2019 / *Accepted:* 23 April 2019 / *Published:* 10 June 2019

Modification of commercial separators with conductive and active barrier layers towards soluble polysulfides is an effective way to combat the shuttle effect and improve the utilization rate of sulfur in lithium-sulfur (Li-S) batteries. Herein, well-dispersed amorphous Ta_2O_5 was chemically grafted onto oxidized multi-walled carbon nanotubes (CNT-O) under mild conditions by a one-pot solvent evaporation method. The prepared Ta_2O_5/CNT-O composite was used as a modified separator layer in a Li-S battery, which combined the advantages of the intertwined structure of conductive CNT-O and the chemisorption ability of Ta_2O_5. Cyclic voltammetry (CV) curves and X-ray photoelectron spectroscopy (XPS) verified the catalytic effect of Ta_2O_5 on the redox reactions during the discharge/charge processes and the strong chemical interactions between polysulfides and Ta_2O_5. Scanning electron microscopy (SEM) images of the modified separators after cycling revealed that the well-dispersed amorphous Ta_2O_5 could immobilize soluble polysulfides through chemical interactions and prevent aggregation of the insoluble products (Li_2S_2, LiS_2 and S_8) during the redox reactions, leading to a uniform redistribution of the sulfur species inside the modification layer, which could ensure the conductivity of the modification layer and high utilization rate of sulfur during long-term cycling processes. A Li-S cell prepared with Ta_2O_5/CNT-O modified separator exhibited a high initial specific capacity of 1230.7 mAh/g at a current density of 0.2 C and stable cycle performance with a decay rate of only 0.11% per cycle over 500 discharge/charge cycles.

Keywords: Lithium Sulfur Battery, Modified Separator, Chemical Grafting, Amorphous Ta_2O_5, Cycle Performance

1. INTRODUCTION

Lithium sulfur (Li-S) batteries are considered one of the most promising rechargeable batteries[1] because of their exceptional theoretical specific energy (1675 mAh/g) and energy density (2600

Wh/kg)[2-4]. However, the commercialization of Li-S batteries has been hindered by the low conductivities of their active materials[5] and the shuttle effects of the soluble polysulfides Li_2S_x (x = 4, 6, 8) formed during the discharge/charge processes[6]. All of the above issues result in the loss of the active material, a low rate performance and a rapid capacity fading[7]. Modifying the separator with a conductive and active barrier layer is one of the promising methods to solve these problems. Since commercial separators are not electron conductors, a thick overlayer consisting of insoluble products (Li_2S_2, LiS_2) precipitates on the separator and cannot be further converted to sulfur (S_8) during the charging process[8], resulting in a low utilization rate of sulfur. Consequently, the specific capacity and cyclic stability of the Li-S battery drops very quickly. Yao[8] et al. reported that, with a 2 μm conductive carbon material (Super C, carbon nanotube) layer on the cathode side of a commercial separator, the formation of the inactive S-related species layer could be prevented, and the initial specific capacity and cyclic stability of the Li-S cell were significantly improved. This research illustrates that a carbon coating on a separator results in a more conductive surface to accommodate the soluble polysulfides Li_2S_x (x = 4, 6, 8) and acts as an upper current collector to accelerate the transport of electrons into the sulfur species.

However, it is not sufficient to only enhance the electronic conductivity of the cathode side, since non-polar carbon materials have poor adsorption abilities towards polar lithium polysulfides[9]. The carbon material-modified separator cannot further inhibit the shuttle effect, which results in a poor rate performance and low Coulombic efficiency. To restrain the shuttle effect, some studies have reported that polar materials, including metal organic frameworks (MOF), chalcogenides and transition metal oxides, which have strong binding interactions with sulfur species, could be used as adsorbents in Li-S cells to inhibit the shuttle effects[10-13]. Among them, transition metal oxides[14-20] have received more attention than other polar materials because of their much stronger binding energies with polysulfides and their flexibility for combining with different carbon materials in Li-S batteries. Therefore, loading transition metal oxides onto carbon materials can be a promising method to improve the electrochemical performance of Li-S batteries, which can not only accelerate electron transfer but also help capture sulfur species with the metal oxides through chemical interactions during the discharge/charge processes. Transition metal oxides, such as MnO[20], ZrO_2[21], La_2O_3[22] and CeO_2[23], loaded onto carbon frameworks have been studied in Li-S batteries and exhibited substantial improvements in the cyclic performance and rate performance. However, most of these transition metal oxides were prepared by complicated procedures under high-temperature conditions and were physically attached to the surface of the carbon materials. The lack of bridging bonds between the carbon lattice and metal oxides limits electron transfer at the interface and greatly reduces the conversion rate of polysulfides captured by the metal oxides during discharge/charge cycling.

To improve the electron transfer capacity of the metal oxide-modified separator, well-dispersed amorphous Ta_2O_5 was chemically grafted onto the surface of CNT-O by a simple one-pot solvent evaporation method. Unlike other metal oxide/carbon composites in the literature[20-23], the facile one-pot solvent evaporation method for fabricating the Ta_2O_5/CNT-O composite under mild conditions allows the amorphous Ta_2O_5 to be distributed more uniformly over the surface of the carbon nanotubes through substitution and hydrolysis reactions between tantalum ethoxide ($Ta(OEt)_5$) and the carboxylic acid groups on CNT-O[24]. The results of the electrochemical tests and physical characterization show

that the Li-S cell prepared with the Ta_2O_5/CNT-O-modified separator had a high specific capacity and stable cyclical performance because of its chemisorption capacity towards the soluble lithium polysulfides and the strong catalytic effect of Ta_2O_5 on the redox reactions during the cycling process, which ensured the good conductivity of the modification layer and a high utilization rate of sulfur during long-term discharge/charge processes. The obvious improvement in the electrochemical performance of the Ta_2O_5/CNT-O modification layer prepared through a one-pot method indicates its potential for practical application in Li-S batteries.

2. EXPERIMENTAL

2.1. Preparation of the Ta_2O_5/CNT-O composite

2.1.1. Multi-walled carbon nanotube oxidation

The mixed acid oxidation method[25] was used to prepare CNT-O by adding 2 g of multi-walled carbon nanotubes to 300 ml of a mixed acid (98% H_2SO_4:68% HNO_3 = 3:1, by volume). The above suspension was ultrasonicated at 37 °C for 2 h and then filtered and washed with deionized water until obtaining a neutral solution. The obtained black filter residue was dried under vacuum at 60 ℃ for 12 h.

2.1.2. Preparation of the Ta_2O_5/CNT-O composite by a solvent evaporation method

The procedure for fabricating the Ta_2O_5/CNT-O composite by using solvent evaporation is shown in Scheme 1[24]. First, 500 mg of CNT-O was added to 20 ml of ethanol and sonicated for 30 min to disperse the CNT-O. An appropriate amount of $Ta(OEt)_5$ was added dropwise to the above suspension, which was then stirred until the solvent had completely evaporated. The residual solid was vacuum-dried at 60 ℃ for 6 h and then ground for 30 min to obtain the Ta_2O_5/CNT-O powder. Through slow evaporation of the solvent, the well-dispersed amorphous Ta_2O_5 loaded onto the surface of the CNT-O was produced by substitution and hydrolysis reactions between $Ta(OEt)_5$ and the carboxylic acid groups on CNT-O. As shown in Scheme 1, Ta_2O_5 was connected to CNT-O through C-O bonds, which was beneficial for obtaining a uniform dispersion of amorphous Ta_2O_5 on CNT-O[24].

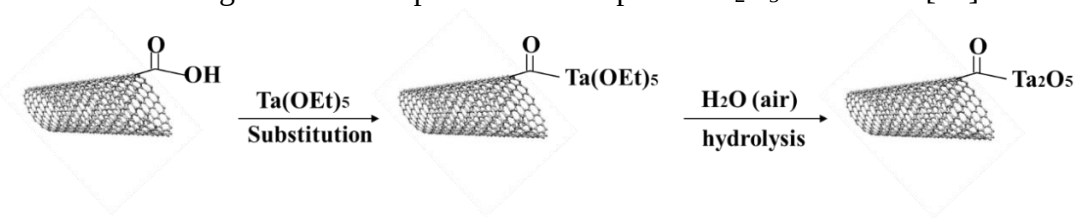

Scheme 1. Fabrication of the Ta_2O_5/CNT-O composite by a facile solvent evaporation method

2.2. Preparation of the Ta_2O_5/CNT-O modified separators and sulfur cathodes

The Ta_2O_5/CNT-O modified separators were fabricated via coating the Ta_2O_5/CNT-O composite onto one side of a commercial separator (Celgard 2325). Specifically, the Ta_2O_5/CNT-O composite was mixed with polyvinylidene fluoride (PVDF) with a weight ratio of 9:1, ground for 30 min and then

dispersed in *N*-methylpyrrolidone (NMP) with continuous vigorous stirring for 24 h to form a slurry. The obtained slurry was coated onto one side of a commercial separator with an automatic coating machine (Shenzhen Kejing, MSK-AFA-SC300). The modified separator was vacuum-dried at 60 ℃ for 12 h and subsequently punched into circular disks with diameters of 19 mm.

The S cathode was prepared in the same way. S_8, Super C and PVDF were dispersed in NMP with a weight ratio of 8:1:1 to obtain a cathode slurry, which was then coated onto Al foil with an automatic coating machine. After being vacuum-dried at 60 ℃ for 12 h, the coated Al foil was punched into 12 mm diameter disks. The mass loading of sulfur on the prepared cathodes was approximately 1.5 mg/cm^2.

2.3. Cell assembly

CR2032 coin cells were assembled in an argon-filled glove box (Mikrouna, Super (1220/750/900)). The lithium foil, S cathode, and commercial separator, with the modified side facing the S cathode, were used as the anode, cathode, and separator, respectively. The electrolyte was composed of 1.0 M lithium bis(trifluoromethanesulfonyl)imide (LiTFSI) and 0.1 M $LiNO_3$ in a mixture of dimethoxyethane (DME) and 1,3-dioxolane (DOL) (1:1, v/v), and the volume of the electrolyte in the cell was 30 μL.

2.4. Electrochemical measurements

The assembled cells were aged for 12 h before the measurements. The cyclic stabilities, specific capacities, and rate performance at different current densities were assessed from discharge/charge measurements by a cell test instrument (Land, CT2001A). The cyclic voltammetry (CV) curves were tested by an electrochemical workstation (Autolab, PGSTAT302N) from 1.7 to 2.8 V at a scan rate of 0.2 mV/s. Electrochemical impedance spectroscopy (EIS) measurements were carried out at a frequency range of 10^{-2} ~ 10^6 Hz. All of the measurements were carried out at room temperature (25 ± 2 °C).

2.5. Physical characterization

The morphologies of CNT-O and the Ta_2O_5/CNT-O composite were obtained by high-resolution transmission electron microscopy (HRTEM) on a JEOL JEM-2010. The morphologies of the modified separators before and after cycling were observed by scanning electron microscopy (SEM) on a JSM-6360 LV at an accelerating voltage of 15 keV. To verify the lithium polysulfide adsorption ability and the chemical states of the amorphous Ta_2O_5 loaded onto CNT-O, X-ray photoelectron spectroscopy (XPS) was employed by a Thermo Scientific ESCALAB 250Xi with a focused monochromatic Al Kα X-ray source. All XPS data were calibrated to the C 1s peak at 284.4 eV. The composition of Ta_2O_5/CNT-O was investigated by a Netzsch STA449F3 TG-DSC analyser in an air atmosphere over a temperature range of 0 ~ 900 ℃ with a heating rate of 5 ℃/min.

3. RESULTS AND DISCUSSION

3.1. Physical characterization of the Ta_2O_5/CNT-O composite

The HRTEM image of CNT-O shows that the tubular structure of the carbon nanotubes after oxidation is not destroyed and that the surface is smooth (Figure 1a). Compared with CNT-O, the HRTEM images of the Ta_2O_5/CNT-O composite (Figure 1b, c) indicate that the surface of the Ta_2O_5/CNT-O composite becomes rough, and substances uniformly loaded onto the carbon nanotubes can be observed. As shown in Figure 1c, the sheet-like structure can be clearly observed with a size of approximately 5 nm. It is preliminarily suspected that the substance loaded onto the surface of CNT-O is amorphous Ta_2O_5[24].

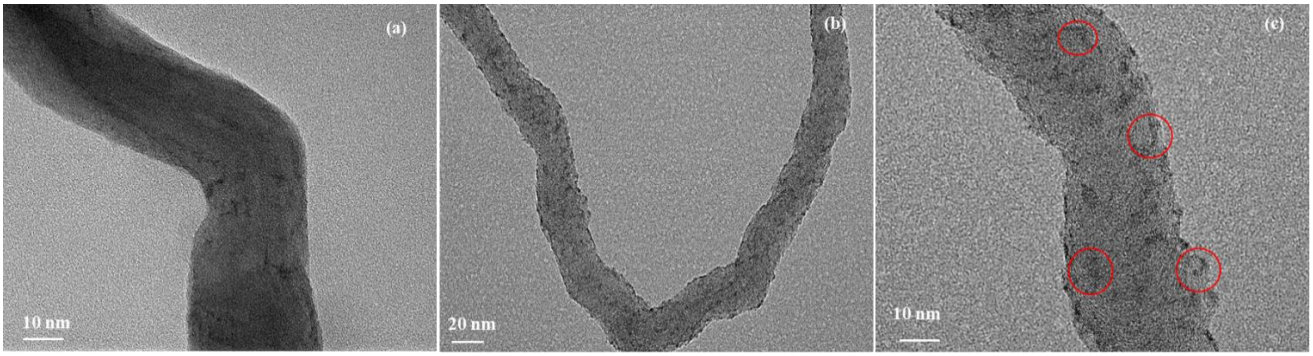

Figure 1. HRTEM images of (a) CNT-O and (b, c) Ta_2O_5/CNT-O.

XPS measurements of CNT-O and the Ta_2O_5/CNT-O composite were then carried out to confirm the identity of the substance loaded onto CNT-O. Figure 2a shows the full XPS spectra of CNT-O and Ta_2O_5/CNT-O, in which the O 1s and C 1s peaks can be detected in the full spectrum of CNT-O in the range of 0~900 eV. In addition to the O 1s peak and the C 1s peak, the XPS full spectrum of Ta_2O_5/CNT-O displays the Ta 4d peak and the Ta 4f peak, proving that the Ta_2O_5/CNT-O composite obtained by the solvent evaporation method contains Ta. To verify the existing form of Ta in the Ta_2O_5/CNT-O composite, the Ta 4f spectrum was analysed. As shown in Figure 2b, the Ta 4f spectrum of Ta_2O_5/CNT-O possesses two predominant peaks at 26.6 eV and 28.5 eV, which can be assigned to Ta $4f_{7/2}$ and Ta $4f_{5/2}$, respectively, corresponding to Ta^{5+} in Ta_2O_5 with a spin energy separation of 1.9 eV[26, 27]. Additionally, the O 1s spectra of CNT-O and Ta_2O_5/CNT-O are displayed in Figure 2c and Figure 2d. As displayed in Figure 2d, the O 1s spectrum of the Ta_2O_5/CNT-O composite possesses a Ta-O peak at 530.9 eV[26, 27], which is consistent with the result of the Ta 4f spectrum. Combining the TEM images and XPS analysis, it can be concluded that amorphous Ta_2O_5 was successfully loaded onto CNT-O. The O 1s spectra of the CNT-O and Ta_2O_5/CNT-O composite both contain peaks that can be assigned to C=O (531.5 eV), C-OH (532.3 eV) and O-C=O (531.6 eV)[28]. However, compared with that of CNT-O, the O-C=O peak area of the Ta_2O_5/CNT-O composite is significantly reduced, while the C=O peak area is significantly increased, indicating that Ta_2O_5 replaces the -OH of the -COOH groups on CNT-O to form Ta_2O_5-C=O, which is consistent with the theoretical analysis in Scheme 1.

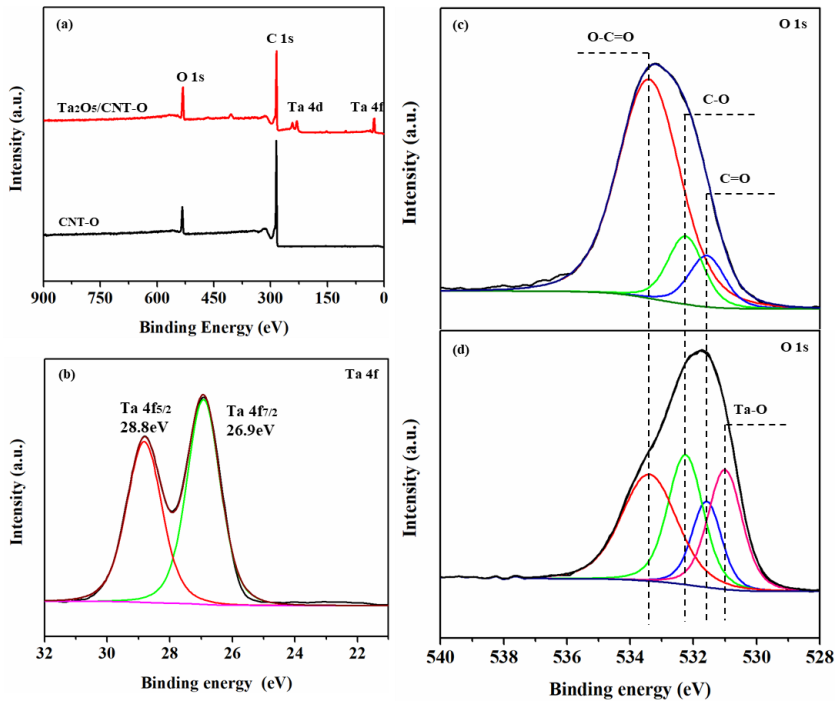

Figure 2. XPS (a) full spectra of CNT-O and Ta_2O_5/CNT-O, (b) the Ta 4f spectrum of Ta_2O_5/CNT-O and the O 1s spectra of (c) CNT-O and (d) Ta_2O_5/CNT-O.

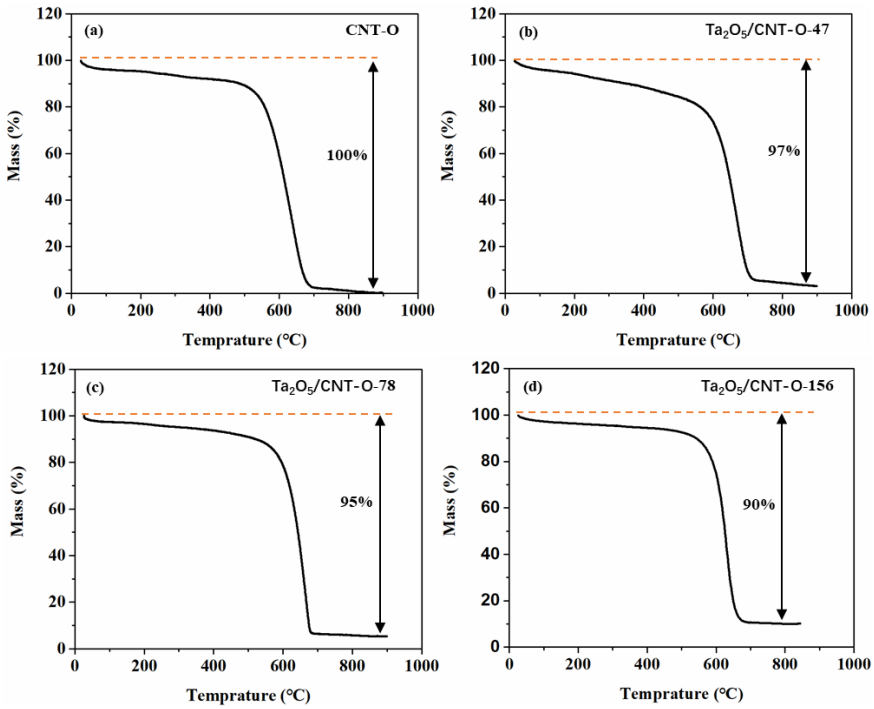

Figure 3. TG curves of CNT-O (a) and the Ta_2O_5/CNT-O composites obtained by adding (b) 47 mg, (c) 78 mg and (d) 156 mg of $Ta(OEt)_5$ to the CNT-O/ethanol suspension during the preparation process.

Three kinds of Ta_2O_5/CNT-O composites with different Ta_2O_5 loading levels (47 mg, 78 mg and 156 mg of $Ta(OEt)_5$ added to the CNT-O/ethanol suspension during the preparation process) were prepared and labelled Ta_2O_5/CNT-O-47, Ta_2O_5/CNT-O-78, and Ta_2O_5/CNT-O-156, respectively. To

obtain the accurate mass percentages of Ta_2O_5 in these three samples, thermogravimetric (TG) tests of CNT-O, Ta_2O_5/CNT-O-47, Ta_2O_5/CNT-O-78, and Ta_2O_5/CNT-O-156 were conducted. Figure 3a shows that CNT-O had burned out when the temperature reached 900 °C. Figure 3b, c, d show that the mass loss is 97%, 95% and 90% when the temperature is increased to 900 °C, which indicates that the mass percentages of Ta_2O_5 in the samples of Ta_2O_5/CNT-O-47, Ta_2O_5/CNT-O-78, and Ta_2O_5/CNT-O-156 are 3%, 5% and 10%, respectively. These three samples are labelled Ta_2O_5/CNT-O-3%, Ta_2O_5/CNT-O-5%, and Ta_2O_5/CNT-O-10%.

3.2. Cycling performance of different modified separators

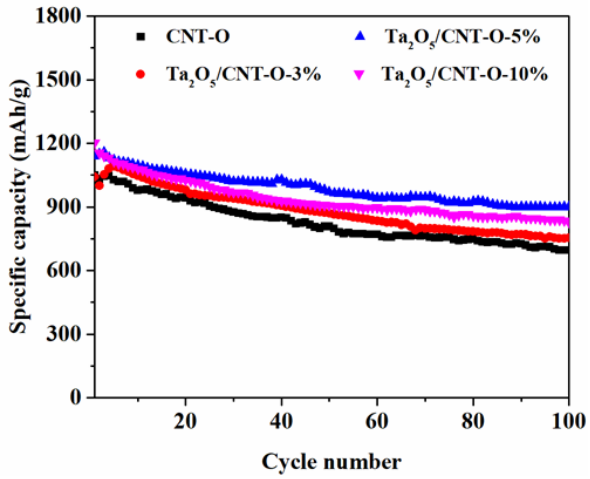

Figure 4. Galvanostatic discharge/charge cycling performance of Li-S cells prepared with CNT-O, Ta_2O_5/CNT-O-3%, Ta_2O_5/CNT-O-5%, and Ta_2O_5/CNT-O-10% modified separators at 0.2 C.

To test the cycling performance of Li-S batteries prepared with different modified separators, CR2032 coin cells were assembled. Figure 4 shows the galvanostatic discharge/charge cycling performance of the Li-S cells prepared with CNT-O, Ta_2O_5/CNT-O-3%, Ta_2O_5/CNT-O-5%, and Ta_2O_5/CNT-O-10% modified separators at a current density of 0.2 C. The cells with Ta_2O_5/CNT-O-3%, Ta_2O_5/CNT-O-5%, and Ta_2O_5/CNT-O-10% modified separators display higher discharge specific capacities during the 100 discharge/charge cycles than that of the CNT-O modified separator, indicating that the amorphous Ta_2O_5 loaded onto CNT-O can help improve the cycling performance of Li-S batteries. However, the Ta_2O_5/CNT-O-3% modified separator shows a lower discharge capacity compared to that of the Ta_2O_5/CNT-O-10% and Ta_2O_5/CNT-O-5% modified separators. Even though the initial specific capacity of the Ta_2O_5/CNT-O-10% modified separator is 1203.4 mAh/g, the capacity decreases rapidly after 10 cycles, showing poor cycling stability. In contrast, the cell prepared with a Ta_2O_5/CNT-O-5% modified separator shows excellent cycling stability. Its initial discharge specific capacity is 1230.7 mAh/g; after 100 cycles, the discharge specific capacity remains at 932.6 mAh/g, showing a capacity retention rate of 75.78%. According to the galvanostatic discharge/charge cycling performance analysis, it can be concluded that the cycling performance of the Li-S cell prepared with the Ta_2O_5/CNT-O-5% modified separator is the best.

3.3. Effect of Ta_2O_5 on the discharge/charge process

3.3.1. Cyclic voltammetry (CV) test

Figure 5 displays the first-cycle CV curves of the cells prepared with CNT-O and Ta_2O_5/CNT-O-5% separators at a scan rate of 0.2 mV/s within the voltage window of 1.7 ~ 2.8 V. All the curves display one broad oxidation peak at approximately 2.4 V in the anodic scan, which reflects the oxidation reactions of Li_2S_n (n = 1 or 2) into Li_2S_n (3<n<8), and then into S_8. There are two reduction peaks at approximately 2.1 V and 2.3 V in the cathodic scan, which correspond to the reduction of S_8 into soluble Li_2S_n (3<n<8) and insoluble Li_2S_n (n = 1 or 2), respectively[29, 30]. As shown in Figure 5, the cathodic and anodic peaks of the Ta_2O_5/CNT-O-5% modified separator are sharper than those of the CNT-O modified separator, which indicates that the amorphous Ta_2O_5 loaded onto CNT-O can help to accelerate the electron/ion transfer processes[14]. In addition, the reduction peaks of the Ta_2O_5/CNT-O-5% modified separator are positively shifted in the cathodic scan, and the oxidation peaks have a negative shift in the anodic scan compared with those of the CNT-O modified separator. These results indicate that Ta_2O_5 can help catalyse the redox reactions of the sulfur species in Li-S batteries, promoting the conversion of the soluble polysulfide lithium Li_2S_n (3<n<8) into insoluble polysulfide Li_2S_n (n = 1 or 2) or S_8, which further inhibits the shuttle effect and improves the utilization of the active materials[29, 31]. The CV results are similar to those from studies on other transition metal oxides, such as Nd_2O_5[17], V_2O_5[18], CeO_2[16, 29] and TiO_2[30].

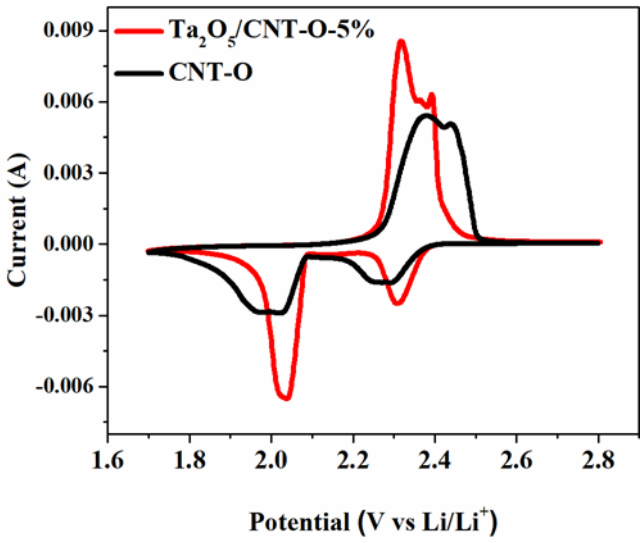

Figure 5. Cyclic voltammetry (CV) curves of Li-S cells prepared with CNT-O and Ta_2O_5/CNT-O-5% modified separators.

3.3.2. Adsorption ability test

To verify the adsorption ability of the amorphous Ta_2O_5 loaded onto CNT-O towards soluble lithium polysulfides, 10 mg of CNT-O and Ta_2O_5/CNT-O-5% were added to a Li_2S_6-DOL/DME solution. After 24 h, as displayed in Figure 6a, the yellow-coloured Li_2S_6 solution (blank) had become

almost transparent for the Ta_2O_5/CNT-O-5% mixture. However, the solution with CNT-O is still yellow. This phenomenon indicates that the amorphous Ta_2O_5 loaded onto CNT-O has a strong adsorption ability towards Li_2S_6. To further confirm the role of Ta_2O_5 during the discharge/charge process, CNT-O and Ta_2O_5/CNT-O-5% modified separators after a 100 cycle test at 0.2 C were separately immersed into 3 ml of DME for 24 h. UV-Vis (Figure 6b) measurements demonstrate that the solution with the Ta_2O_5/CNT-O-5% separator shows a lower absorption peak intensity for Li_2S_6 than that of the CNT-O modified separator. The inset of Figure 6b shows the colour change of the solutions with CNT-O and Ta_2O_5/CNT-O-5% separators after the 100 cycle test. The colour of the solution with the CNT-O separator is much darker than that of the Ta_2O_5/CNT-O-5% separator, which is in good agreement with the UV-Vis results. The UV-Vis results reveal that the amorphous Ta_2O_5 loaded onto CNT-O can effectively inhibit the diffusion of the soluble polysulfide into the electrolyte. There are two reasons for this phenomenon: (1) the strong adsorption ability of Ta_2O_5 towards lithium polysulfides and (2) the redox catalytic effect of Ta_2O_5, which help accelerate the conversion of soluble polysulfides into insoluble polysulfides and sulfur.

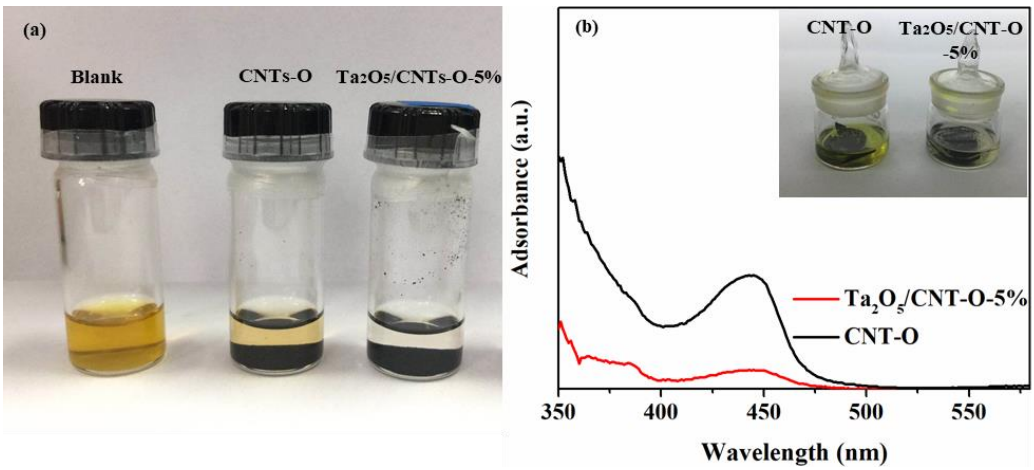

Figure 6. (a) Digital photographs of the polysulfide simulated adsorption tests for CNT-O and Ta_2O_5/CNT-O-5%, (b) UV-Vis absorption spectra of the DME solutions with CNT-O and Ta_2O_5/CNT-O-5% modified separators after 100 cycles (Inset in Figure 6b shows the colour change of the DME solutions with 100 cycle tests of the CNT-O and Ta_2O_5/CNT-O-5% modified separators after standing for 24 h).

3.3.3. XPS analysis of the modified separators after cycling

To further explore the chemisorption and catalytic effects of the amorphous Ta_2O_5 on the redox reactions of the polysulfides, XPS measurements of the CNT-O and Ta_2O_5/CNT-O-5% modified separators after 100 cycles at 0.2 C were carried out. Figure 7a, b display the S 2p spectra of the CNT-O and Ta_2O_5/CNT-O-5% modified separators. As presented in Figure 7a, the peaks at 170.8 eV, 169.7 eV and 167.4 eV are attributed to the sulfur species present in the electrolyte salt, LiTFSI. The peak at 165.3 eV are assigned to S_8. The peaks at 164 eV and 162.9 eV are assigned to the S-S bonds and Li-S

bonds of Li_2S_n (3<n<8), respectively[31, 32, 33]. All of the S 2p peak positions of the Ta_2O_5/CNT-O-5% modified separator are the same as those of the CNT-O modified separator except for the peak of the S-S bonds of Li_2S_n (3<n<8), which shows a positive shift of 0.3 eV compared with the peak of the CNT-O modified separator (Figure 7b). Furthermore, the Ta 4f spectrum of the 100 cycle tested Ta_2O_5/CNT-O-5% modified separator possesses two predominant peaks at 26.6 eV and 28.5 eV (Figure 7c), corresponding to Ta^{5+} in Ta_2O_5 with a spin energy separation of 1.9 eV[26, 27], which shows a negative shift of 0.3 eV compared with the locations of the Ta 4f spectral peaks of the Ta_2O_5/CNT-O-5% composite before cycling (Figure 2b). The shifts of these peak positions are believed to be induced by the strong binding interaction between Li_2S_n (3<n<8) and Ta_2O_5[30], proving the strong chemisorption ability of Ta_2O_5 towards the lithium polysulfides. In addition, as shown in Figure 7b, the peaks assigned to soluble Li_2S_n (3<n<8) in the spectrum of the Ta_2O_5/CNT-O-5% modified separator are much weaker than those in the spectrum of the CNT-O modified separator. Notably, S_8 is the main sulfur element in the Ta_2O_5/CNT-O-5% separator after cycling, which indicates that more Li_2S_n (3<n<8) is converted into S_8 as a result of the catalytic effect of the Ta_2O_5 loaded onto CNT-O during the charging process.

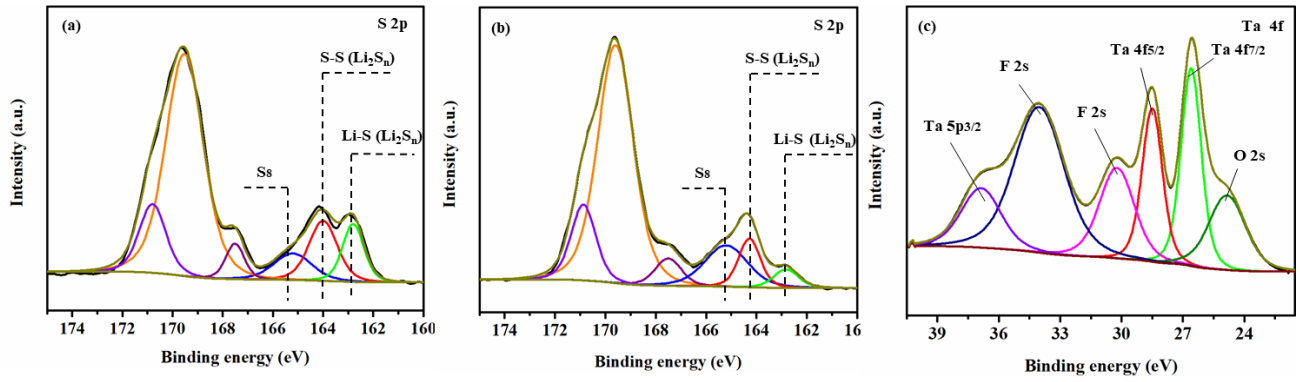

Figure 7. S 2p spectra of the (a) CNT-O and (b) Ta_2O_5/CNT-O-5% modified separators and (c) Ta 4f spectrum of the Ta_2O_5/CNT-O-5% modified separator after 100 discharge/charge cycles at 0.2 C.

3.3.4. SEM analysis of the modified separators after cycling

The intertwined array of carbon nanotubes can be observed in the SEM image of the separator modified by the Ta_2O_5/CNT-O-5% composite (Figure 8a), which can help accelerate the physical adsorption of the lithium polysulfides. From the cross-sectional SEM image (Figure 8b), the thickness of the Ta_2O_5/CNT-O-5% modified separator can be determined to be approximately 5 μm. The surface and cross-sectional morphologies of the CNT-O modified separator are the same as those of the Ta_2O_5/CNT-O-5% modified separator. However, as displayed in Figure 8c, the surface of the CNT-O modified separator becomes rough after 100 cycles at 0.2 C, which is caused by the nonuniform deposition of insoluble sulfur species (S_8, Li_2S_2 and Li_2S) inside the CNT-O modified layer produced by the reduction and oxidation of the soluble polysulfides dissolved in the electrolyte. Compared with the CNT-O modified separator, the surface of the Ta_2O_5/CNT-O-5% modified separator is much smoother after 100 cycles (Figure 8d). This phenomenon is mainly due to the strong adsorption ability of the

amorphous Ta_2O_5 uniformly loaded onto CNT-O towards the lithium polysulfides, which can adsorb and immobilize soluble polysulfides inside the modified coating layer to some extent, accelerating the uniform deposition of the insoluble sulfur species inside the modification layer during the redox reactions. To summarize, the SEM images of the CNT-O and Ta_2O_5/CNT-O-5% modified separator after cycling reveal that the well-dispersed amorphous Ta_2O_5 can help promote the uniform redistribution of sulfur species inside the modified separator.

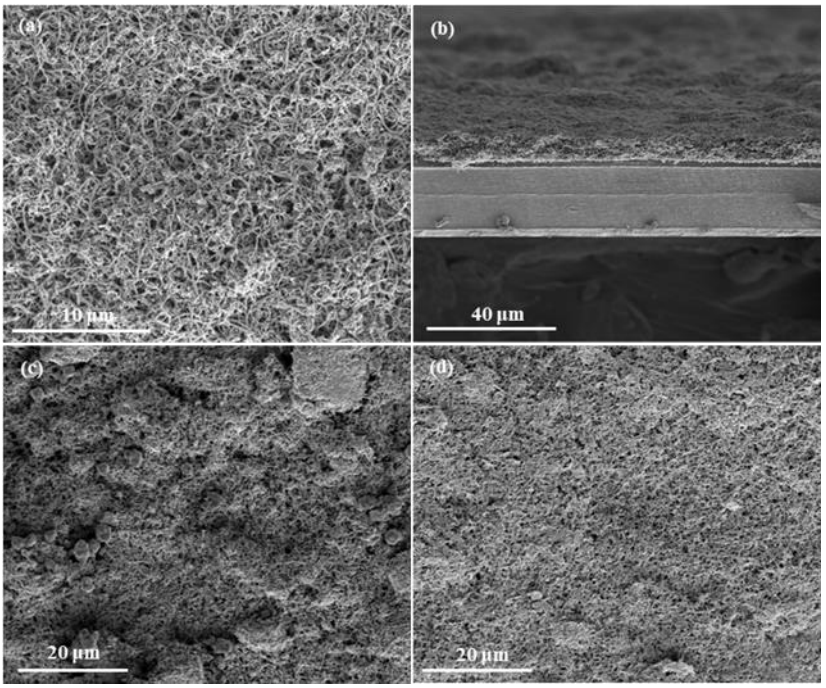

Figure 8. (a) Surface and (b) cross-sectional SEM images of the Ta_2O_5/CNT-O-5% modified separator and SEM images of the (c) CNT-O and (d) Ta_2O_5/CNT-O-5% modified separator after a 100 cycle test at 0.2 C.

3.4. Electrochemical tests

To further understand the function of the amorphous Ta_2O_5 inside the modified separator coating, EIS analysis of the Li-S batteries prepared with CNT-O and Ta_2O_5/CNT-O-5% modified separators after 100 cycles at 0.2 C was carried out (Figure 9a). Nyquist plots of the modified separators after 100 cycles consist of a semicircle in the high-frequency range, which reflects the resistance of the solid-electrolyte interface (SEI) film (R_s), a semicircle in the medium-high-frequency range, corresponding to the charge transfer resistance (R_{ct}), and an inclined line in the low-frequency range, reflecting the Warburg impedance (W_0) [34, 35]. As shown in Figure 9a, after cycling, the resistance of the SEI film (R_s) of the cell prepared with the Ta_2O_5/CNT-O-5% modified separator is smaller than that of the cell with the CNT-O modified separator. To some extent, this result implies that the amorphous Ta_2O_5 loaded onto CNT-O can help inhibit the soluble polysulfides from passing through the separator and reacting with lithium metal because of its chemisorption ability towards the polysulfides. Additionally, compared with

the cell prepared with the CNT-O modified separator, the charge transfer resistance (R_{ct}) of the cell with the Ta_2O_5/CNT-O-5% modified separator after cycling is much smaller, which agrees well with the SEM images of the CNT-O and Ta_2O_5/CNT-O-5% modified separators after cycling, suggesting that well-dispersed amorphous Ta_2O_5 can help inhibit the agglomeration of the insoluble active sulfur species during the redistribution process, thereby ensuring the conductivity of the modified layer and improving sulfur utilization during long-term cycling.

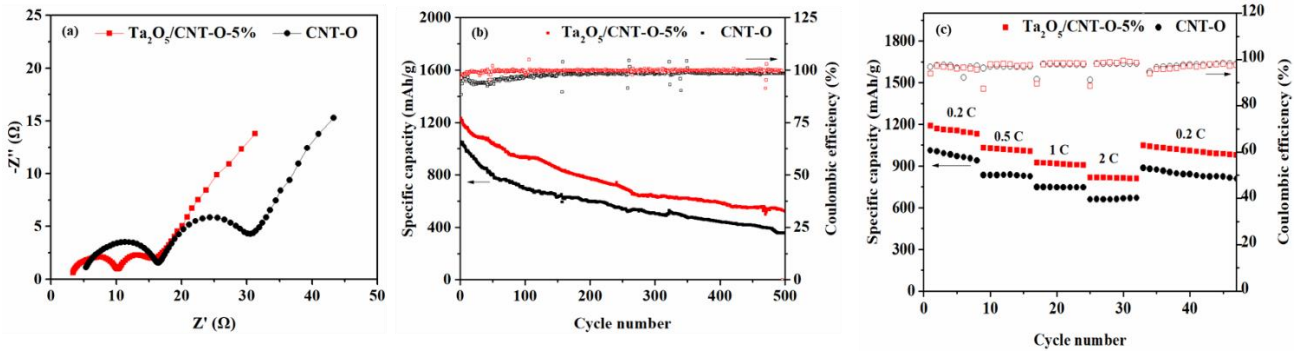

Figure 9. (a) Nyquist plots of the Li-S batteries prepared with CNT-O and Ta_2O_5/CNT-O-5% modified separators after a 100 cycle test at 0.2 C, (b) long-term cycling performance at 0.2 C and (c) rate performance of Li-S cells prepared with CNT-O and Ta_2O_5/CNT-O-5% modified separators.

To demonstrate the advantageous electrochemical performance of the cell with a Ta_2O_5/CNT-O-5% modified separator, long-term cycling and rate performance tests were conducted between 1.7 ~ 2.8 V. Figure 9b shows the long-term cycling performance at 0.2 C of the coin cells prepared with separators modified by CNT-O and Ta_2O_5/CNT-O-5%. The initial discharge specific capacity of the cell prepared with a CNT-O modified separator is 1049.4 mAh/g, and a capacity of only 357 mAh/g is obtained after 500 cycles, representing a decay rate of 0.13% per cycle. In contrast, the initial specific capacity of the cell with the Ta_2O_5/CNT-O-5% modified separator is 1230.7 mAh/g and delivers a specific capacity of 523 mAh/g after 500 discharge/charge cycles, a decay rate of only 0.11% per cycle, which indicates the low capacity fading and long life span of the Ta_2O_5/CNT-O-5% modified separator. Obviously, the stable cycling performance of the cell prepared with the Ta_2O_5/CNT-O-5% modified separator is attributed to the amorphous Ta_2O_5, which helps inhibit the shuttle effect and accelerates the uniform distribution of sulfur species inside the modification layer during the long-term cycling process. Figure 9c shows the rate performance of the Li-S cells prepared with CNT-O and Ta_2O_5/CNT-O-5% modified separators. The discharge specific capacities of the cell with the CNT-O modified separator are 1011.6 mAh/g, 833.6 mAh/g, 747.3 mAh/g and 660.1 mAh/g at current densities of 0.2 C, 0.5 C, 1 C and 2 C, respectively. When the current density is returned to 0.2 C, the discharge specific capacity returns to 885.4 mAh/g. Compared with the cell prepared with the CNT-O modified separator, the cell with the Ta_2O_5/CNT-O-5% modified separator displays better rate performance, and the corresponding discharge specific capacities are 1190 mAh/g, 1030 mAh/g, 925 mAh/g and 818 mAh/g. When the current density returns to 0.2 C, the discharge specific capacity returns to 1049 mAh/g. The rate performance analysis demonstrates that the cell with the Ta_2O_5/CNT-O-5% modified separator possesses an excellent rate performance because of the chemisorption and catalytic effect of Ta_2O_5. Notably, compared with

previous literatures reported other modified separators for Li-S batteries, the Ta_2O_5/CNT-O-5% modified separator in this work delivers much better or at least comparable cycling performance and longer life span (Table 1).

Table 1. The cycle performance comparisons of Ta_2O_5/CNT-O-5% modified separator for Li-S batteries with other modified separators from previous reported literatures.

Sample	Sulfur content of cathode (%)	Sulfur mass loading (g/cm^2)	Current density (C)	Cycles	Innitial capacity (mAh/g)	Reversible capacity (mAh/g)	Capacity decay per cycle (%)
Ta_2O_5/CNT-O-5% separator	80	1.5	0.2	500	1230	523	0.11
MCNT coated separator[8]	60	1.5~2	0.2	150	1100	760	0.2
KB/MnO separator[20]	64	1.5~2	1	200	1059	901	0.07
Hollow La_2O_3 coated separator[14]	64	1.5	1	200	996	720	0.14
Al_2O_3-coated separator[36]	60	1.6	0.2	50	967	593.4	0.77
MoO_3@CNT Interlayer[37]	60	1	0.3	200	1425	755	0.24

4. CONCLUSION

Well-dispersed amorphous Ta_2O_5 were chemically grafted onto the surface of CNT-O under mild conditions by a one-pot method through the substitution and hydrolysis reactions between $Ta(OEt)_5$ and the carboxylic acid groups on CNT-O, and the fabricated Ta_2O_5/CNT-O composite was successfully used as a modified separator layer in a Li-S battery. The adsorption simulation tests and XPS spectra revealed the strong chemisorption ability of the amorphous Ta_2O_5 towards soluble polysulfides. The positive shifts of the reduction peaks and negative shifts of the oxidation peaks in the CV curves proved the catalytic effect of Ta_2O_5 on the redox reactions. The SEM images and Nyquist plots showed that the well-dispersed amorphous Ta_2O_5 could promote the uniform redistribution of insoluble sulfur species inside the modification layer, which increased the utilization rate of the active material and ensured the conductivity of the modified coating layer during long-term cycling. The electrochemical test results showed that the Ta_2O_5/CNT-O-5% separator exhibited a high discharge specific capacity, low capacity fade and long life span. The strategy for chemically grafting a transition metal oxide onto the surface of carbon nanotubes provides a new and effective method for the practical application of Li-S batteries.

CONFLICTS OF INTEREST

There are no conflicts to declare.

ACKNOWLEDGMENTS
We acknowledge the National Key R&D Program of China (Grant No. 2017YFB0307502 and Grant No. 2017YFB0307500), the 111 Project of China (No. B08021), the Collaborative Innovation Centre for Petrochemical New Materials, Anqing, Anhui, P.R. China (No.246011), and the Shanghai Pujiang Program (No.18PJ1402000).

References

1. R. Tripathi, S.M. Wood, M.S. Islam and L.F. Nazar, *Energy Environ. Sci.,* 6 (2013) 2257.
2. Z.W. Seh, Y.M. Sun, Q.F. Zhang and Y. Cui, *Chem. Soc. Rev.,* 45 (2016) 5605.
3. M. Wild, L. O'Neill, T. Zhang, R. Purkayastha, G. Minton, M. Marinescu and G.J. Offer, *Energy Environ. Sci.,* 8 (2015) 3477.
4. P.G. Bruce, S.A. Freunberger, L.J. Hardwick and J.M. Tarascon, *Nat. Mater.,* 11 (2012) 19.
5. X.L. Ji and L.F. Nazar, *J. Mater. Chem.,* 20 (2010) 9821.
6. Y.B. He, Y. Qiao and H.S. Zhou, *Dalton Trans.,* 47 (2018) 6881.
7. Z. Yuan, H.J. Peng, T.Z. Hou, J.Q. Huang, C.M. Chen, D.W. Wang, X.B. Cheng, F. Wei and Q. Zhang, *Nano Lett.,* 16 (2016) 519.
8. H.B. Yao, K. Yan, W. Li, G. Zheng, D. Kong, Z.W. Seh, V.K. Narasimhan, Z. Liang and Y. Cui, *Energy Environ. Sci.,* 7 (2014) 3381.
9. Q. Pang, D. Kundu, M. Cuisinier and L.F. Nazar, *Nat. Commun.,* 5 (2014) 4759.
10. Z.W. Seh, W.Y. Li, J.J. Cha, G.Y. Zheng, Y. Yang, M.T. McDowell, P.C. Hsu and Y. Cui, *Nat. Commun.,* 4 (2013) 1331.
11. L. Ma, S.Y. Wei, H.L. Zhuang, K.E. Hendrickson, R.G. Hennig and L.A. Archer, *J. Mater. Chem. A,* 3 (2015) 19857.
12. J.M. Zheng, J. Tian, D.X. Wu, M. Gu, W. Xu, C.M. Wang, F. Gao, M.H. Engelhard, J.G. Zhang, J. Liu and J. Xiao, *Nano Lett.,* 14 (2014) 2345.
13. S.S. Zhang and D.T. Tran, *J. Mater. Chem. A,* 4 (2016) 4371.
14. X. Qian, D. Zhao, L. Jin, X. Shen, S. Yao, D. Rao, Y. Zhou and X.M. Xi, *Mater. Res. Bull.,* 94 (2017) 104.
15. G. Xu, Q.B. Yan, S. Wang, A. Kushima, P. Bai, K. Liu, X. Zhang, Z. Tang and J. Li, *Chem. Sci.,* 8 (2017) 6619.
16. X. Qian, L. Jin, L. Zhu, S. Yao, D. Rao, X. Shen, X. Xi, K. Xiao and S. Qin, *RSC Adv.,* 6 (2016) 111190.
17. Y. Tao, Y. Wei, Y. Liu, J. Wang, W. Qiao, L. Ling and D. Long, *Energy Environ. Sci.,* 9 (2016) 3230.
18. Y. Guo, Y. Zhang, Y. Zhang, M. Xiang, H. Wu, H. Liu and S. Dou, *J. Mater. Chem. A,* 6 (2018) 19358.
19. Y. Zhang, Y. Zhao, A. Yermukhambetova, Z. Bakenov and P. Chen, *J. Mater. Chem. A,* 1 (2013) 295.
20. X.Y. Qian, L. Jin, D. Zhao, X.L. Yang, S.W. Wang, X.Q. Shen, D.W. Rao, S.S. Yao, Y.Y. Zhou and X.M. Xi, *Electrochim. Acta,* 192 (2016) 346.
21. C.Y. Wan, W.L. Wu, C.X. Wu, J.X. Xu and L.H. Guan, *RSC Adv.,* 5 (2015) 5102.
22. F.G. Sun, J.T. Wang, D.H. Long, W.M. Qiao, L.C. Ling, C.X. Lv and R. Cai, *J. Mater. Chem. A,* 1 (2013) 13283.
23. X.Y. Qian, L.N. Jin, L. Zhu, S.S. Yao, D.W. Rao, X.Q. Shen, X.M. Xi, K.S. Xiao and S.B. Qin, *RSC Adv.,* 6 (2016) 111190.
24. Y. Shin, J.Y. Kim, C. Wang, J.F. Bonnet and K.Scott. Weil, *Surf. Sci.,* 603 (2009) 2290.

25. L. Wang, L. Zhang, X. Xue, G. Ge and X. Liang, *Nanoscale,* 4 (2012) 3983.
26. M. Hellwig, A. Milanov, D. Barreca, J.L. Deborde, R. Thomas, M. Winter, U. Kunze, R.A. Fischer and A. Devi, *Chem. Mater.,* 19 (2007) 6077.
27. G. Zhu, T. Lin, H. Cui, W. Zhao, H. Zhang and F. Huang, *ACS Appl. Mater. Interfaces,* 8 (2016) 122.
28. R. Larciprete, S. Gardonio, L. Petaccia and S. Lizzit, *Carbon,* 47 (2009) 2579.
29. L.B. Ma, R.P. Chen, G.Y. Zhu, Y. Hu, Y.R. Wang, T. Chen, J. Liu and Z. Jin, *ACS Nano,* 11 (2017) 7274.
30. G.M. Zhou, Y.B. Zhao, C.X. Zu and A. Manthiram, *Nano Energy,* 12 (2015) 240.
31. Y. Diao, K. Xie, S.Z. Xiong and X.B. Hong, *J. Electrochem. Soc.,* 159 (2012) A1816.
32. D.B. Babu, K. Giribabu and K. Ramesha, *ACS. Appl. Mater. Interfaces,* 10 (2018) 19721.
33. Y. Diao, K. Xie, S.Z. Xiong and X.B. Hong, *J. Power Sour*ces*,* 235 (2013) 181.
34. I.J. Gordon, S. Genies, G.S. Larbi, A. Boulineau, L. Daniel and M. Alias, *J. Power Sources,* 307 (2016) 788.
35. I.J. Gordon, S. Grugeon, A. Debart, G. Pascaly and S. Laruelle, *Solid State Ion.,* 237(2013) 50.
36. Z.Y. Zhang, Y.Q. Lai, Z. Zhang, K. Zhang and J. Li, *Electrochim. Acta,* 129 (2014) 55.
37. L. Y. Luo, X.Y. Qin, J.X. Wu, G.M. Liang, Q. Li, M. Liu, F.Y. Kang, G.H. Chen and B.H. Li, *J. Mater. Chem. A,* 6 (2018): 8612.